Mon. Not. R. Astron. Soc. **267**, 1020–1034 (1994)

Reconstructing the linear power spectrum of cosmological mass fluctuations

J. A. Peacock[1] and S. J. Dodds[2]

[1]*Royal Observatory, Blackford Hill, Edinburgh EH9 3HJ*
[2]*Institute for Astronomy, University of Edinburgh, Blackford Hill, Edinburgh EH9 3HJ*

Accepted 1993 November 24. Received 1993 November 24; in original form 1993 August 11

ABSTRACT

We describe an attempt to reconstruct the initial conditions for the formation of cosmological large-scale structure, under the assumption of gravitational instability in a Gaussian density field. Information on the power spectrum of the primordial fluctuations is provided by a variety of autocorrelation and cross-correlation analyses on samples of different classes of galaxy and galaxy clusters. These results differ from the desired linear power spectrum because of three modifying effects: bias, non-linear evolution and redshift-space distortions. We show how the latter two effects can be corrected for analytically, allowing the linear mass spectrum to be recovered provided that the bias is independent of scale for a given class of galaxy. We argue that this is a good assumption for large scales, which is well verified in practice.

We apply this method to eight independent data sets, and obtain excellent agreement in the estimated linear power spectra for wavelengths $\lambda \gtrsim 10\,h^{-1}$Mpc, given the following conditions. First, the relative bias factors for Abell clusters, radio galaxies, optical galaxies and *IRAS* galaxies must be in the ratios $b_A : b_R : b_O : b_I = 4.5 : 1.9 : 1.3 : 1$, to within 6 per cent rms. Secondly, the data require a significant degree of redshift-space distortion: $\Omega^{0.6}/b_I = 1.0 \pm 0.2$. Thirdly, low values of Ω and bias are disfavoured because non-linear evolution would spoil the agreement in shape between galaxy and cluster power spectra. The amplitude of the preferred linear power spectrum is only weakly dependent on Ω and agrees well at large wavelengths with the normalization demanded by the *COBE* data for a scale-invariant primordial spectrum, provided that $\Omega = 1$ and gravity-wave anisotropies are negligible. In this case, the shape of the spectrum is extremely well described by a CDM transfer function with an apparent value of the fitting parameter $\Omega h = 0.25$. Tilted models, for which inflation requires a large gravity-wave contribution to the *COBE* data, predict too little power at 100-Mpc wavelengths.

Key words: galaxies: clustering – cosmology: theory – large-scale structure of Universe.

1 INTRODUCTION

The simplest hypothesis for the origin of the large-scale structure of the Universe is that it is the result of the operation of gravitational instability on small initial density perturbations. On grounds of economy, these are often assumed to have the random-phase character common in noise processes, and hence to form a Gaussian random field. This has been the standard picture for structure formation for the half century since the pioneering studies of Lifshitz, given added motivation more recently by inflationary theories in which the initial perturbations are supplied by quantum fluctuations at early times.

If this picture is correct, the only quantity needed for a complete statistical description of the cosmological density field is the power spectrum of the fluctuations at some early time (or its linear-theory extrapolation to the present). Observationally, much progress has been made in recent years towards the goal of determining the power spectrum, fulfilling the programme outlined by Peebles (1973). New generations of deep redshift surveys have allowed the clustering of various classes of galaxy to be determined up to the contribution from wavelengths of several hundred Mpc. In parallel, new analysis techniques have been developed in order to extract the long-wavelength portion of the power spectrum more sensitively (e.g. Feldman, Kaiser & Peacock 1994 [FKP] and references therein).

The intention of this paper is to compare various recent determinations of galaxy clustering, and to see if there exists a single consistent picture for the underlying mass fluctuations. It is an updated version of a previous attempt in this direction (Peacock 1991), but with several important improvements in

addition to a great increase in quantity of data. In essence, there are three filters that cause the observed clustering properties of galaxies to depart from the desired linear mass power spectrum.

(i) Non-linear evolution. On small scales, perturbation theory fails and the mass power spectrum departs in a complicated way from a linear extrapolation of the initial conditions.

(ii) Redshift-space effects. Because 3D data sets use redshift as a radial coordinate, the apparent density field that results is distorted through the existence of peculiar velocities. Even for perfect data, the redshift-space power spectrum is not the same as that in real space.

(iii) Bias. The fact that different species of galaxy follow the mass distribution with different degrees of fidelity is a major problem in relating observations to theory. To correct for bias in principle requires a detailed model for how the effect arises.

None of these effects was handled very thoroughly in previous work. The issue of bias is the most difficult, and is really only tractable on large scales where the degree of bias can be assumed constant. It is now possible to have a better idea of where this approximation is valid, and we discuss this issue in Section 2. Previously, non-linear distortions were either ignored or treated by comparing non-linear data with an evolved N-body model. However, thanks to the insight of Hamilton et al. (1991; HKLM), it is possible to correct the data for the effects of non-linearities. We discuss their method in Section 3 and give a number of generalizations. Redshift-space distortions have usually been treated by a simple scaling of amplitude analysed by Kaiser (1987), but this is inapplicable on small scales. We give an improved analysis in Section 4.

Given a method for treating the practical distortions of power spectra, there are two possible approaches. There is an honourable tradition which states that it is better to apply any corrections to the theory under test, and to compare the modified model with the raw data. Nevertheless, we shall do the opposite and estimate the linear spectrum by correcting the data. This has two advantages: no model is needed, and the power spectrum can be found empirically; by comparing the various estimates, we can then see directly if all data sets are consistent with each other. In Section 5, we assemble the most recent power-spectrum data and apply the above tools to deduce the linear power spectrum. This empirical reconstruction is compared with a variety of a priori models in Section 6, and the main points of the paper are summarized in Section 7.

2 GALAXY AND CLUSTER CORRELATIONS IN GAUSSIAN MODELS

2.1 Evidence for Gaussian fluctuations

Since a good part of the analysis in this paper rests on the assumption of a Gaussian density field, we should start by considering the evidence that this is a good approximation.

The evidence has to be gathered on large scales, because non-linear evolution inevitably induced non-Gaussian statistics on small scales, whatever the initial statistics. The most direct test was carried out by FKP, who looked at the distribution of power measured for individual modes in a power-spectrum analysis of the *IRAS* QDOT redshift survey. For a Gaussian field, such modes should have power values that are independently exponentially distributed. This was found to be the case out to the limit of the statistics – powers of about 10 times the mean. This is not a complete test of the Gaussian hypothesis: it is equivalent to asking in real space whether the one-point density distribution is Gaussian. Further information is provided by higher-order k-space correlations which test for independence of the modes. Nevertheless, it is worth recalling that there have been suggestions that even this lowest-order test is badly violated. On the basis of a pencil-beam redshift survey, Broadhurst et al. (1990) and Szalay et al. (1991) have suggested that there is gross non-Gaussian behaviour on large scales, based on the existence of strong quasi-periodic power at a few wavelengths. There is no need to repeat here the counter-arguments given by Kaiser & Peacock (1991); it should suffice to note that the QDOT sample is deep enough that it encompasses several of the suggested periods in a large number of independent directions, yet no non-Gaussian signature is detected.

Any initial Gaussian nature of the field is completely erased on very small scales, but on intermediate scales the field develops a skewness which can be analysed perturbatively (Peebles 1980). The observed degree of skewness appears to be in accord with this prediction (Gaztañaga 1992; Bouchet et al. 1993), which gives further support to the Gaussian hypothesis. This is not a definitive test, since most bias mechanisms will induce skewness; what is observed is a mixture of this effect with primordial skewness, plus the effects of gravitational evolution. Nevertheless, simple Gaussian models without a strong degree of bias do account for the data well.

A variety of other tests have been suggested, including the topology of isodensity surfaces (Hamilton, Gott & Weinberg 1986; Coles & Plionis 1991; Moore et al. 1992) and the one-point distribution of the velocity field (Nusser & Dekel 1993; Kofman et al. 1994). It is fair to say that none of these methods has produced any evidence against primordial Gaussian statistics. However, as usual in statistics, it is necessary to choose the null hypothesis with care. It is certainly the case that not all tests are necessarily very powerful; the central limit theorem means that a variety of non-Gaussian processes may yield nearly Gaussian behaviour in experiments where limited resolution averages over different regions of space (Scherrer 1992). Thus some of the more popular models based on topological singularities (strings, textures etc.) may still be allowed by existing data (e.g. Gooding et al. 1992). However, it will be interesting to see such theories confronted with the FKP result, particularly as such statistics will become more demanding as data sets increase in size.

For the present, it is enough to note that there is empirical reason to believe that the statistics of the large-scale density field are close to Gaussian. If this is so, then there are consequences for the clustering of galaxy systems, as discussed below. As we will see, these predictions are verified in practice, which is one further piece of supporting evidence for the Gaussian picture.

2.2 Bias in galaxy and cluster correlations

In a Gaussian model, the correlations of different classes of galaxy system can be directly related to the underlying density field, with the power spectra being proportional on large scales:

$$\Delta^2(k) = b^2\,\Delta^2_{\rm mass}(k). \quad (1)$$

Here and below, we shall use a dimensionless notation for the power spectrum designed to minimize uncertainties from differing Fourier conventions. In words, Δ^2 is the contribution to the fractional density variance per bin of $\ln k$; in the convention of Peebles (1980), this is

$$\Delta^2(k) \equiv \frac{{\rm d}\sigma^2}{{\rm d}\ln k} = \frac{V}{(2\pi)^3}\,4\pi k^3\,|\delta_k|^2. \quad (2)$$

The justification for the above relation is the assumption, introduced by Kaiser (1984), Peacock & Heavens (1985) and Bardeen et al. (1986; BBKS), that the sites of massive objects such as clusters can be identified at early times as high peaks in the linear density field. Such a scheme might be termed Lagrangian bias, and b is called a bias parameter. This is rather sloppy: biased galaxy formation usually means the situation where light does not trace mass in the Universe, but clusters would still be more correlated than the mass even if the galaxy distribution followed the mass exactly. However, this usage is too firmly embedded in the literature to make it worth fighting; we will therefore describe the enhanced correlations of clusters as bias.

As the density field evolves, the initial statistical clustering in Lagrangian space is supplemented as dynamics moves objects from their initial sites. Owing to the equivalence principle, all objects move in the same way, so that the overall observed clustering in Eulerian space is

$$1 + \delta_{\rm Euler} = (1 + \delta_{\rm Lagrange})\,(1 + \delta_{\rm dynamics}). \quad (3)$$

In the linear regime, we therefore have

$$\delta_{\rm Lagrange} = (b - 1)\delta_{\rm dynamics}. \quad (4)$$

Bond & Couchman (1988) showed how this decomposition could be used to compute exact total correlations, under the assumption that the dynamical evolution obeyed the Zeldovich (1970) approximation. Mann, Heavens & Peacock (1993) applied this method to the calculation of cluster correlations. In practice, the statistical contribution tends to dominate for scales larger than the filter size used to define clusters (a few Mpc); the cluster distribution has not undergone strong dynamical evolution, and most clusters are close to their original sites.

Although the idea of Lagrangian bias was borrowed by BBKS from its cluster origins and applied as a model for biased galaxy formation, it may be more fruitful to think of galaxy bias in a purely Eulerian way, where the density of galaxies is some function of the final mass density. This has long been advocated by Einasto and collaborators, with galaxy formation being suppressed in low-density regions (Einasto, Jôeveer & Saar 1980). More recently, studies of the operation of dissipation in numerical simulations have produced a more direct physical justification for relating the galaxy and mass density fields through a single non-linear function (Cen & Ostriker 1992).

These contrasting views of the origin of cluster and galaxy bias lead to rather different approaches when attempting to use clustering data to infer the mass fluctuations. For clusters, the statistical bias is dominant, and we may assume that the clusters reflect mainly the initial conditions. Conversely, it is reasonable to believe that galaxies come close to tracing the mass. Many studies have indicated that different classes of galaxy follow the same 'skeleton' of voids, filaments, walls and clusters, while differing most markedly in regions of high density (e.g. Babul & Postman 1990; Strauss et al. 1992). This last effect may not be so important: despite having densities differing by factors of close to 10 in rich clusters, we shall see below that *IRAS* and optical galaxies have bias factors within about 30 per cent of each other. This is analogous to the findings of Cen & Ostriker (1992): even though their model has a highly non-linear dependence of galaxy density on mass density for high densities, the power spectra are proportional on most scales, even down to the point where $\Delta^2(k) \sim 1$. In any case, it is important to keep in mind that we are not interested in exactly how a given class of galaxy does or does not follow the density field: a variety of different bias schemes could give the same galaxy power spectrum, even though the light distributions would be model dependent.

The above discussion motivates the assumptions that we shall use below to make estimates of the linear power spectrum. We shall adopt the extreme approximations that the cluster distribution contains information only about the linear power spectrum, whereas the galaxy distribution mainly measures the non-linear density field:

$$\Delta^2_{\rm C} = b^2_{\rm C}\Delta^2_{\rm L}, \quad (5)$$

$$\Delta^2_{\rm G} = b^2_{\rm G}\Delta^2_{\rm NL}. \quad (6)$$

A further way of understanding this distinction is to consider the following illustrative model, in which we populate the Universe with identical spherical protocluster perturbations. At some critical time, these will turn round and virialize, producing a large excess of small-scale power in the non-linear density field. However, at this time, the cluster centres will still be weakly perturbed: the existence of the small-scale power is what allows us to say that clusters are present, but there is no reason to expect this power to manifest itself in many close pairs of cluster centres. Ultimately, our hypothesis must submit to the test of numerical simulation, but for the present it should certainly be closer to the truth to say that clusters respond to the linear power spectrum, rather than to the non-linear one.

Although the above bias factors are calculable given a specific bias model, we shall treat them as unknowns to be determined from the data. It is clear that the assumption of constant bias factors cannot be exact, and will certainly break down at small scales. To some extent, the domain of validity can be found empirically, by seeing whether it is possible to make a consistent picture in this way from all the available data. In practice, we shall use data at wavenumbers $k \lesssim 0.6\,h\,{\rm Mpc}^{-1}$, i.e. wavelengths $\lambda \gtrsim 10\,h^{-1}{\rm Mpc}$ (as usual, $h \equiv H_0/100\,{\rm km\,s^{-1}Mpc^{-1}}$), so we are only dealing with the large-scale mass distribution.

There is a third way in which the mass power spectrum may be inferred, which is to use cross-correlation data from two catalogues, in addition to the respective autocorrelations. In this case, it is not so obvious whether we measure more nearly the linear or non-linear correlations. In practice, we shall use data on large enough scales that the distinction will not be so important; we therefore assume a relation to linear theory

$$\Delta^2_{\rm CG} = b_{\rm C}b_{\rm G}\Delta^2_{\rm L}. \quad (7)$$

This provides a useful consistency test of our assumptions: the cluster-galaxy cross-correlation should be the geometrical mean of the separate autocorrelations.

3 NON-LINEAR EVOLUTION OF POWER SPECTRA

To implement the above assumptions requires some way of relating linear and non-linear power spectra; until recently, this would have required N-body modelling. However, in a marvelous piece of alchemy, Hamilton et al. (1991; HKLM) gave a universal analytical formula for accomplishing the linear $\leftrightarrow$ non-linear mapping. The conceptual basis of their method can be understood with reference to the spherical collapse model. For $\Omega = 1$ (the only case they considered), a spherical clump virializes at a density contrast of order 100 when the linear contrast is of order unity. The trick now is to think about the density contrast in two distinct ways. To make a connection with the statistics of the density field, the correlation function $\xi(r)$ may be taken as giving a typical clump profile. What matters for collapse is that the integrated overdensity reaches a critical value, so one should work with the volume-averaged correlation function $\bar{\xi}(r)$. A density contrast of $1+\delta$ can also be thought of as arising through collapse by a factor $(1+\delta)^{1/3}$ in radius, which suggests that a given non-linear correlation $\bar{\xi}_{\rm NL}(r_{\rm NL})$ should be thought of as resulting from linear correlations on a linear scale

$$r_{\rm L} = [1 + \bar{\xi}_{\rm NL}(r_{\rm NL})]^{1/3} r_{\rm NL}. \tag{8}$$

This is one part of the HKLM procedure. The second part, having translated scales as above, is to conjecture that the non-linear correlations are a universal function of the linear ones:

$$\bar{\xi}_{\rm NL}(r_{\rm NL}) = f_{\rm NL}[\bar{\xi}_{\rm L}(r_{\rm L})]. \tag{9}$$

The asymptotics of the function can be deduced readily. For small arguments $x \ll 1$, $f_{\rm NL}(x) \simeq x$; the spherical collapse argument suggests $f_{\rm NL}(1) \simeq 10^2$. Following collapse, $\bar{\xi}_{\rm NL}$ depends on scale factor as a^3 (stable clustering), whereas $\bar{\xi}_{\rm L} \propto a^2$; the large-$x$ limit is therefore $f_{\rm NL}(x) \propto x^{3/2}$. HKLM deduced from numerical experiments that the exact coefficient is

$$f_{\rm NL}(x) \rightarrow 11.68\, x^{3/2} \tag{10}$$

and obtained a numerical fit that interpolated between these two regimes, in a manner that empirically showed negligible dependence on power spectrum.

To use this method in the present application, we need two generalizations: we need to make the method work with power spectra, and we need the analogous results with $\Omega \neq 1$. In principle, the translation between $\bar{\xi}(r)$ and $\Delta^2(k)$ is straightforward, but it is not so easy to obtain stable numerical results. One route is to use the relations between $\bar{\xi}(r)$ and $\xi(r)$:

$$\bar{\xi}(r) = \frac{3}{r^3} \int_0^r \xi(x)\, x^2\, {\rm d}x, \tag{11}$$

$$\xi(r) = \frac{{\rm d}\,[r^3\, \bar{\xi}(r)]}{{\rm d}[r^3]}, \tag{12}$$

followed by the Fourier relations between $\xi(r)$ and $\Delta^2(k)$:

$$\xi(r) = \int_0^\infty \Delta^2(k)\, \frac{\sin kr}{kr}\, \frac{{\rm d}k}{k}, \tag{13}$$

$$\Delta^2(k) = \frac{2k^3}{\pi} \int_0^\infty \xi(r)\, \frac{\sin kr}{kr}\, r^2\, {\rm d}r. \tag{14}$$

This approach is not so attractive. To obtain the non-linear power spectrum from the linear one requires two numerical integrations, followed by differentiation, followed by one further integration. It is possible to do a little better by manipulating the above equations to relate $\Delta^2(k)$ and $\bar{\xi}(r)$ directly:

$$\bar{\xi}(r) = \int_0^\infty \Delta^2(k)\, \frac{{\rm d}k}{k}\, \frac{3}{(kr)^3} [\sin kr - kr \cos kr], \tag{15}$$

$$\Delta^2(k) = \frac{2k^3}{3\pi} \int_0^\infty \bar{\xi}(r)\, r^2\, {\rm d}r\, \frac{1}{(kr)} [\sin kr - kr \cos kr], \tag{16}$$

where the last relation holds provided that $\bar{\xi}(r) \rightarrow 0$ faster than r^{-2} at large r (i.e. a spectrum which asymptotically has $n > -1$, a valid assumption for spectra of practical interest). This looks better, since there are now only two integrations required, and furthermore efficient methods exist for dealing with integrations with sin and cos weightings in the integrand. However, because the window function consists of the difference of two such terms, life is still not so easy: evaluation of the two parts of the integral separately gives a result as a difference of two large numbers, which is thus generally of low accuracy. The most satisfactory practical procedure seems to be a mixture of the two possibilities: (i) evaluate a table of $\bar{\xi}_{\rm L}(r)$ values for a given linear power spectrum by evaluating the oscillatory integral directly; (ii) transform to a table of $\bar{\xi}_{\rm NL}(r)$ values using the HKLM procedure; (iii) fit splines to the result and differentiate to get $\xi_{\rm NL}(r)$; (iv) Fourier transform to get $\Delta^2_{\rm NL}(k)$. The accuracy of the result can be improved in the final step by transforming $\xi_{\rm NL}(r) - \xi_{\rm L}(r)$, which vanishes rapidly at large r, and then adding $\Delta^2_{\rm L}(k)$ to the answer.

The above process is still rather time-consuming and inelegant; it would be much better to make the HKLM method work directly in terms of power spectra, and this is usually possible. The main idea is that $\bar{\xi}(r)$ can often be thought of as measuring the power at some effective wavenumber: it is obtained as an integral of the product of $\Delta^2(k)$, which is often a rapidly rising function, and a window function which cuts off rapidly at high k. The answer can be approximated by replacing the exact window function by the Gaussian which is equivalent to second order in k:

$$\bar{\xi}(r) = \Delta^2(k_{\rm eff}), \tag{17}$$

$$k_{\rm eff} = \left[\frac{([n+1]/2)\,!}{2}\right]^{1/(n+3)} \frac{\sqrt{10}}{r}, \tag{18}$$

where n is the effective power-law index of the power spectrum. This approximation is within a few per cent of the exact integration provided that $n \lesssim 0$. The effective wavenumber is insensitive to n, and is within 20 per cent of $2.4/r$ over the range $-2 < n < 0$. In most circumstances, it is therefore an excellent approximation to use the HKLM formulae directly to scale wavenumbers and powers:

$$\Delta^2_{\rm NL}(k_{\rm NL}) = f_{\rm NL}[\Delta^2_{\rm L}(k_{\rm L})], \tag{19}$$

$$k_{\rm L} = [1 + \Delta^2_{\rm NL}(k_{\rm NL})]^{-1/3} k_{\rm NL}. \tag{20}$$

Even better, it is not necessary that the number relating $1/r$ and $k_{\rm eff}$ be a constant over the whole spectrum. All that matters is that the number can be treated as constant over the limited range $r_{\rm NL}$ to $r_{\rm L}$. This means that the deviations of the above formulae from the exact transformation of the HKLM procedure

are only noticeable in cases where the power spectrum deviates markedly from a smooth monotonic function, or where either the linear or non-linear spectra are very flat ($n \lesssim -2$). Even this is not obviously a problem, since the HKLM procedure itself is not exact and does not work so well for flat spectra, $n \lesssim -2$ (A.S. Hamilton, private communication). Our approximation is illustrated in Fig. 1, which shows the result of non-linear evolution on spectra with and without a short-wavelength cutoff. Whether the HKLM method actually applies to the first situation is an interesting question which we hope to investigate elsewhere. Other cases where our approximation would fail include power spectra with the oscillations characteristic of pure baryon models. However, since the data studied here reveal no trace of such sharp features in the power spectrum, we may use the direct approximation for the non-linear evolution of the power spectrum with confidence.

It remains to generalize the result from the $\Omega = 1$ model considered by HKLM. This can be done partly analytically. The argument that leads to the $f_{\rm NL}(x) \propto x^{3/2}$ asymptote in the non-linear transformation is just that linear and non-linear correlations behave as a^2 and a^3 respectively following collapse. If collapse occurs at high redshift, then $\Omega = 1$ may be assumed at that time, and the non-linear correlations still obey the a^3 scaling to low redshift. All that has changed is that the linear growth is suppressed by some Ω-dependent factor $g(\Omega)$. It then follows that the large-x asymptote of the non-linear function is

$$f_{\rm NL}(x) \rightarrow 11.68\,[g(\Omega)]^{-3}\,x^{3/2}. \qquad (21)$$

According to Carroll, Press & Turner (1992), the growth factor may be approximated almost exactly by

$$g(\Omega) = \frac{5}{2}\Omega_{\rm m}\left[\Omega_{\rm m}^{4/7} - \Omega_{\rm v} + (1+\Omega_{\rm m}/2)(1+\Omega_{\rm v}/70)\right]^{-1}, \qquad (22)$$

where we have distinguished matter (m) and vacuum (v) contributions to the density parameter explicitly. We shall generally use Ω without a subscript to mean $\Omega_{\rm m}$ hereafter.

To interpolate between the expected non-linear asymptote and the linear regime, numerical experiments are necessary. We therefore wrote a PM N-body code, which was used to evolve a variety of initial spectra to a final state of given $\Omega_{\rm m}$ and $\Omega_{\rm v}$; typically 64^3 particles and a 128^3 mesh were used. At a later stage of the investigation, we were able to check our results with the superior resolution provided by the AP^{3}M code of Couchman (1991). It was also possible to compare with low-density cold dark matter (CDM) models published by Davis et al. (1985) and Kauffmann & White (1992). Our conclusion is that a near-universal behaviour analogous to that of HKLM does appear to exist for low-density models, at least for the linear spectra with power-law indices $-2 < n < 0$ that we were able to test. We have produced the following fitting formula for the generalized $f_{\rm NL}$. This is designed to match the HKLM expression almost exactly in the $\Omega = 1$ limit, and to describe the main features of the alterations encountered in low-density models. The accuracy is approximately 10 per cent in terms of the deduced linear power $\Delta_{\rm L}^2$ corresponding to a given $\Delta_{\rm NL}^2$, over the range $0.3 \lesssim g(\Omega) \lesssim 1$.

$$f_{\rm NL}(x) = x\left[\frac{1 + 0.2\beta x + (Ax)^{\alpha\beta}}{1 + ([Ax]^{\alpha}g^3(\Omega)/[11.68x^{1/2}])^{\beta}}\right]^{1/\beta}, \qquad (23)$$

where the parameters are $A = 0.84[g(\Omega)]^{0.2}$, $\alpha = 2/[g(\Omega)]$, and $\beta = 2g(\Omega)$. This fit says that the transition region between the linear and non-linear regimes is dominated by an $f_{\rm NL} \propto x^{1+\alpha}$ power law, which becomes very steep for low-density models. This steepening has long been familiar from N-body models, and the apparent power-law nature of the spectrum can been used as an argument against low-density models. We shall end up making a rather similar argument here.

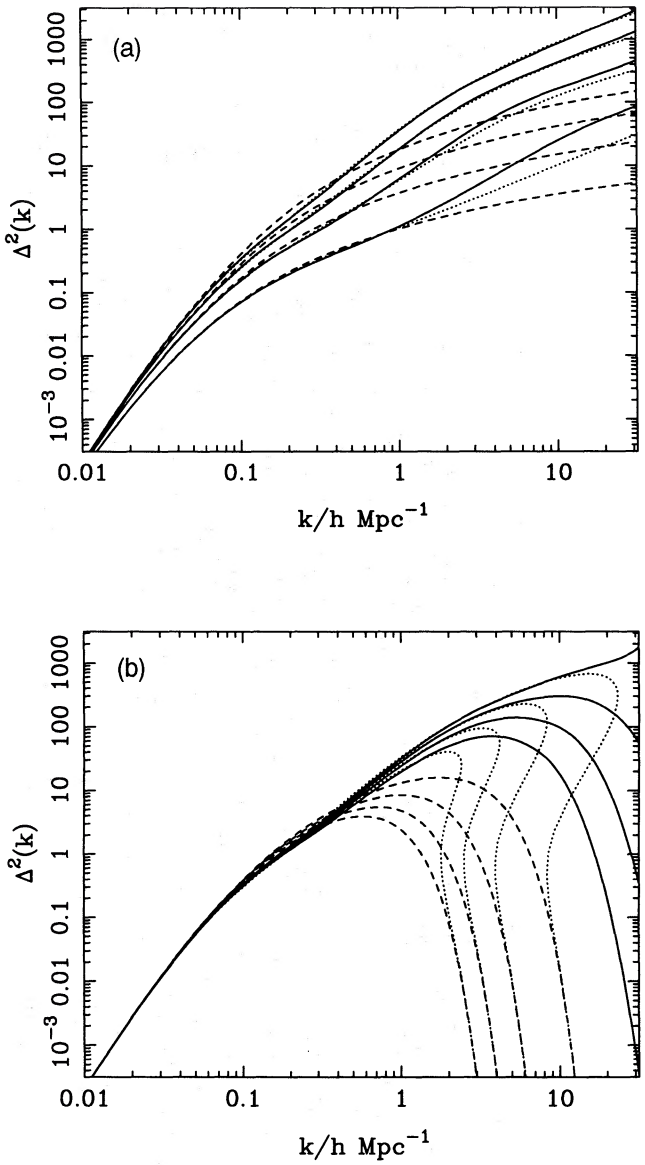

Figure 1. The non-linear evolution of power spectra according to the HKLM method, and the approximate direct alternative presented here. The dashed lines show the input linear power spectra, the solid lines show the result of numerically integrating the HKLM method and the one-step solution is shown dotted. Panel (a) shows a variety of *COBE*-normalized CDM models (with $\Omega h = 0.2$, 0.3, 0.4, 0.5); while (b) shows Ωh=0.5 CDM filtered with different Gaussian windows ($R_{\rm f} = 0.25$, 0.5, 0.75, 1 h^{-1} Mpc), approximating the effect of warm dark matter. As expected, our method fails at very high k, where the linear CDM spectra become very flat and the linear WDM spectra cutoff, but is otherwise excellent. Note that the effect of the WDM cutoff is only felt at very large k: WDM is not the explanation for the shape of the power spectrum around $k = 0.1h$.

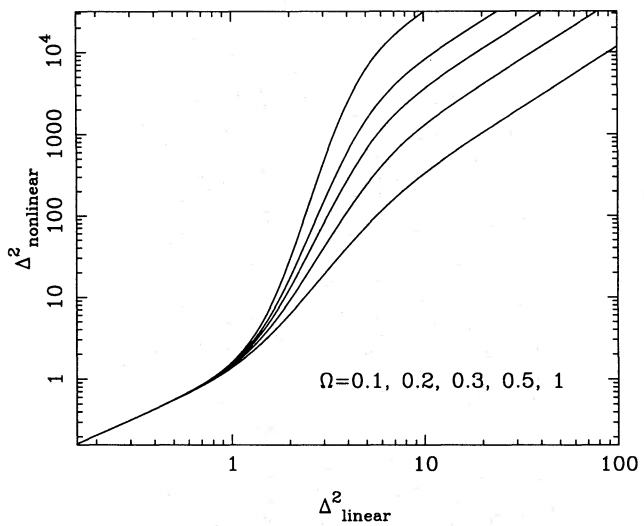

Figure 2. The generalization of the HKLM function relating non-linear power to linear power (or $\bar{\xi}$, as in the original method). The lowest curve is the original HKLM function for $\Omega = 1$; low densities give a greater non-linear response. We show the fitting formula for open models only, but what matters in general is just the Ω-dependent linear growth suppression factor.

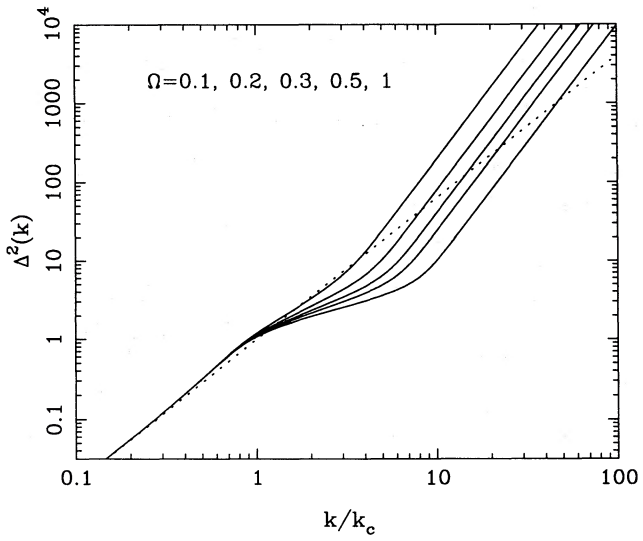

Figure 3. The inverse of the generalized HKLM procedure, as applied to a power-law power spectrum (shown dotted) $\Delta^2(k) = (k/k_c)^{1.8}$ (in correlation-function terms, $r_0 = 0.945/k_c$). Open models with $\Omega = 1$, 0.5, 0.3, 0.2, 0.1 are considered. Note that the effects of non-linearities in this case are rather small for high densities, but for low densities the required linear initial conditions are very flat for $k \gtrsim k_c$. This flat case is one where our approximate inversion of the HKLM procedure will not be perfect (cf. Fig. 1); nevertheless, any errors will be small in comparison with the systematic feature in the power spectrum required around $\Delta^2 \sim 1$. It clearly requires something of a conspiracy to achieve a scale-free non-linear spectrum in a low-density model.

It is useful to have an analytical expression for the inverse function, and the following agrees with the exact inverse of our formula to within a typical maximum error of a few per cent over the range of interest:

$$f_{\rm NL}^{-1}(y) = y\left[\frac{1+(By^{\gamma-1/3}[g^3(\Omega)/11.68]^{2/3})^{\delta}}{1+0.2\delta y+(By^{\gamma})^{\delta}}\right]^{1/\delta}, \qquad (24)$$

where $B = 0.96[g(\Omega)]^{0.07}$, $\gamma = 1.03 - 0.39[g(\Omega)]^{0.5}$, and $\delta = 5[g(\Omega)]^{0.3}$. A plot of the Ω-dependent non-linear function is shown in Fig. 2. We show only models with zero vacuum energy, since the above reasoning shows that all that matters is the linear growth-suppression factor $g(\Omega)$. Note that, for spatially flat vacuum-dominated models, the growth suppression is rather more modest (roughly $g(\Omega) = \Omega^{0.2}$) than in models with zero vacuum energy (roughly $g(\Omega) = \Omega^{0.7}$). Our results (and those of HKLM) apply only to initial conditions with Gaussian statistics. It is an interesting question to what extent the method will also apply to non-Gaussian models, and we hope to investigate this elsewhere. Some idea of the likely degree of universality may be gained from the non-Gaussian models studied by Weinberg & Cole (1992). They found that the non-linear power spectrum was very similar for a range of initial models, with the exception only of those that were strongly skew-negative. It therefore seems likely that mildly non-Gaussian models such as cosmic strings should be treated correctly by the method we have given.

We now have the required means of deducing the initial conditions that correspond to a given observed non-linear mass spectrum. As an example, we show in Fig. 3 the initial conditions required to create the canonical correlation function $\bar{\xi}(r) = (r/r_0)^{1.8}$; i.e. $\Delta^2(k) = (k/k_c)^{1.8}$, where $k_c = 1.058/r_0$. For low-density models, the initial conditions require an enormous 'bite' to be taken out of the spectrum for k between k_c and several times k_c. The reconstructed spectrum tends to be very flat and close to $\Delta^2(k) = 1$ over a large range of wavenumber. Conversely, for $\Omega = 1$ the effects of non-linearities are not very severe in this case until we reach $\Delta^2(k) \gtrsim 10$. These differences will be important when we come to linearize the observed data.

4 REDSHIFT-SPACE DISTORTIONS

With the exception of surveys where angular data are deprojected to obtain an estimate of the spatial power spectrum, three-dimensional clustering data generally involve redshift surveys where the radii are distorted by peculiar velocities. There are two effects to consider. On large scales, a linear analysis should be valid and we have the anisotropic effect noted by Kaiser (1987):

$$\delta_k \rightarrow b\,\delta_k\,(1 + f\mu^2/b), \qquad (25)$$

where μ is the cosine of the angle between the wavevector and the line of sight. The function $f(\Omega) \simeq \Omega^{0.6}$ is the well-known velocity-suppression factor due to Peebles, which is in practice a function of $\Omega_{\rm m}$ only, with negligible dependence on the vacuum density (Lahav et al. 1991). The anisotropy arises because mass flows from low-density regions on to high-density sheets, and the apparent density contrast of the pattern is thus enhanced in redshift space if the sheets lie near the plane of the sky. If we average this anisotropic effect by integrating over a uniform distribution of μ, the net boost to the power spectrum is

$$|\delta_k|^2 \rightarrow b^2 |\delta_k|^2 \left(1 + \frac{2}{3}[f/b] + \frac{1}{5}[f/b]^2\right). \quad (26)$$

On small scales, this is not valid. The main effect here is to reduce power through the radial smearing due to virialized motions and the associated 'finger-of-God' effect. This is hard to treat exactly because of the small-scale velocity correlations. A simplified model was introduced by Peacock (1992) in which the small-scale velocity field is taken to be an incoherent Gaussian scatter with 1D rms dispersion σ. This turns out to be quite a reasonable approximation, because the observed pairwise velocity dispersion is a very slow function of separation, and is all the better if the redshift data are afflicted by significant measurement errors (which should be included in σ). This model is just a radial convolution, and so the k-space effect is

$$\delta_k \rightarrow \delta_k \exp[-k^2\mu^2\sigma^2/2]. \quad (27)$$

This effect in isolation gives an average isotropic factor of

$$|\delta_k|^2 \rightarrow |\delta_k|^2 \frac{\sqrt{\pi}}{2} \frac{\mathrm{erf}\,(k\sigma)}{k\sigma} \quad (28)$$

and produces only mild damping (one power of k at large k).

Some workers (e.g. Fisher et al. 1992; Kofman, Gnedin & Bahcall 1993) have combined the above two effects simply by multiplying the two power correction factors to achieve a total distortion. However, this is not correct: both terms are anisotropic in k space and they interfere before averaging: $\langle A^2B^2\rangle \neq \langle A^2\rangle\langle B^2\rangle$. For the present paper, it is also interesting to consider the case of cross-correlation where each of two catalogues gives a different measure of the same underlying density field. The model for the effect in k space of cross-correlation is then the product of two separate factors of the above form:

$$|\delta_k|^2 \rightarrow b_1 b_2 |\delta_k|^2 (1 + f\mu^2/b_1)(1 + f\mu^2/b_2) \times \exp[-k^2\mu^2(\sigma_1^2 + \sigma_2^2)/2]. \quad (29)$$

The overall effect is obtained by averaging over μ, and looks more complicated than it really is:

$$|\delta_k|^2 \rightarrow b_1 b_2 |\delta_k|^2 \, G(y, \alpha_1, \alpha_2), \quad (30)$$

where

$$y^2 \equiv k^2(\sigma_1^2 + \sigma_2^2)/2, \quad (31)$$

$$\alpha \equiv f(\Omega)/b, \quad (32)$$

$$G(y, \alpha_1, \alpha_2) = \frac{\sqrt{\pi}}{8} \frac{\mathrm{erf}\, y}{y^5} [3\alpha_1\alpha_2 + 2(\alpha_1 + \alpha_2)y^2 + 4y^4] - \frac{\exp(-y^2)}{4y^4} [\alpha_1\alpha_2(3 + 2y^2) + 2(\alpha_1 + \alpha_2)y^2]. \quad (33)$$

This simplifies a little in the case of autocorrelations, where indices 1 and 2 are equivalent. The interesting aspect of this formula is that the linear boost is lost at large k, where the result is independent of Ω (as is obvious from the anisotropic form: the main contribution at large k comes from small μ). The true damping at large k is thus more severe than would be obtained by multiplying the power corrections prior to angular averaging. The simulations of Gramann, Cen & Bahcall (1993) show a good level of agreement with the above formula in the autocorrelation case. The result is reassuringly insensitive to the assumed form for the small-scale velocity distribution function; if we take an exponential instead of a Gaussian, we find the same result at small k:

$$G(y, \alpha_1, \alpha_2) \simeq \left(1 + \frac{\alpha_1 + \alpha_2}{3} + \frac{\alpha_1\alpha_2}{5}\right) - \left(\frac{1}{3} + \frac{\alpha_1 + \alpha_2}{5} + \frac{\alpha_1\alpha_2}{7}\right) y^2, \quad (34)$$

and the large-y limit becomes $G \rightarrow \pi/(2^{3/2}y)$ instead of $G \rightarrow \pi^{1/2}/(2y)$.

In practice, the relevant value of σ to choose is approximately $1/\sqrt{2}$ times the pairwise dispersion $\sigma_\parallel$ seen in galaxy redshift surveys. According to the most recent compilation of velocity results by Mo, Jing & Börner (1993b), this corresponds to the figure (adopted hereafter) of

$$\sigma \simeq 300 \,\mathrm{km\,s^{-1}}. \quad (35)$$

To this, we should add in quadrature any errors in measured velocities. The relatively low value of this dispersion is of course a significant problem for some high-density models. Gramann et al. (1993) argue that redshift-space power spectra of CDM models fit observation very well, mainly because the predicted pairwise dispersion is so high in these models. As we shall see below, such an unrealistically large dispersion would spoil the agreement between data sets in real and in redshift space.

5 POWER-SPECTRUM RECONSTRUCTION

5.1 Data

We now apply the above tools to some of the more recent results on the clustering power spectrum. We shall consider eight distinct sets of data, which fall into several distinct classes.

(i) Real-space clustering of galaxies. Baugh & Efstathiou (1993) have applied a deprojection procedure to the angular clustering of the APM galaxy survey to infer the non-linear power spectrum of optically selected galaxies without redshift-space distortions. This paper considers the large-scale power spectrum, and we have thus used the APM data at $k < 1\,h\,\mathrm{Mpc}^{-1}$ only. To allow comparison with other data sets, we have also set a lower limit of $k > 0.015\,h\,\mathrm{Mpc}^{-1}$.

(ii) Redshift-space clustering of galaxies. We consider three data sets: FKP for *IRAS* galaxies (the QDOT sample); Loveday et al. (1992) for the Stromlo/APM survey; Vogeley et al. (1992) for the CfA survey. The last paper quotes results for two separate subsets; we have adopted a straight mean of the two sets of data. We have not used the *IRAS* data of Fisher et al. (1993), which are systematically lower than those of FKP. As discussed by FKP, this seems most likely to be a local sampling effect. In any case, it is the deeper QDOT sample used by FKP which also appears in cross-correlation analyses (see iv below).

(iii) Redshift-space clustering of groups and clusters of galaxies. We use the power spectrum for $R \geq 1$ Abell clusters from Peacock & West (1992) and also radio galaxies from Peacock & Nicholson (1991), on the assumption that the strongly enhanced clustering of these latter objects may be attributed to their location in moderately rich environments.

(iv) We also use the cross-correlation between *IRAS* galaxies and Abell clusters or radio galaxies from Mo, Peacock & Xia (1993a).

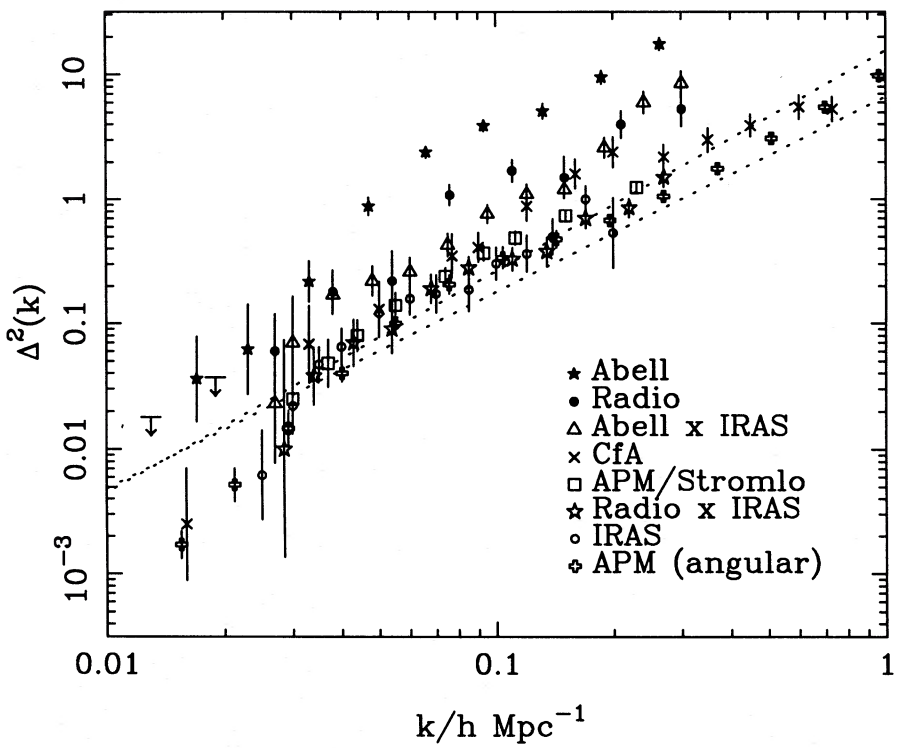

Figure 4. The raw power-spectrum data used in this analysis. All data with the exception of the APM power spectrum are in redshift space. The two lines shown for reference are the transforms of the canonical real-space correlation functions for optical and *IRAS* galaxies ($r_0 = 5$ and 3.78 h^{-1} Mpc and slopes of 1.8 and 1.57 respectively).

Not all of the above data are available directly in power-spectrum form. In cases where what is published is a cell variance or a measure of $\bar{\xi}(r)$, we have used the notion of an effective wavenumber, as discussed above and in Peacock (1991). The treatment of errors requires some discussion. Only FKP give a full realistic error covariance matrix for their data; the other data sets give errors ranging from Poisson estimates to field-to-field errors, but with no discussion of the independence of the measurements at different k. For consistency, we have therefore used a fraction of the FKP data, spaced widely enough to be roughly independent. Any imprecision in this procedure, plus unrecognized systematics, will become apparent when the various data sets are compared with each other.

The raw power-spectrum data are plotted in Fig. 4. There is a wide range of power measured, ranging over perhaps a factor 20 between the real-space APM galaxies and the rich Abell clusters. We now have to see to what extent these measurements are all consistent with one Gaussian power spectrum for mass fluctuations.

5.2 Implications for bias and Ω

The reconstruction analysis has available eight data sets containing 91 distinct $k-\Delta^2$ pairs. The modelling has available five free parameters in the form of Ω and the four bias parameters for Abell clusters, radio galaxies, optical galaxies and *IRAS* galaxies (b_A, b_R, b_O, b_I). We optimized the model by making independent determinations of $\Delta_L^2(k)$ for each data set and then comparing them. This was done in practice by dividing the range $0.01 < k < 0.1\ h\,\mathrm{Mpc}^{-1}$ into 20 bins, and evaluating a weighted mean power and a χ^2 for each bin. The likelihood of the model is given in terms of the summed χ^2 values:

$$\mathscr{L} \propto \exp -\chi^2/2. \tag{36}$$

At this stage, the question arises of whether the errors are realistic, which may be judged from whether the overall χ^2 matches the number of degrees of freedom: in fact, it does not. A procedure that ensures the required match is to add some constant rms error ϵ in quadrature to the existing errors. In practice,

$$\epsilon = 23 \text{ per cent} \tag{37}$$

is required for the best-fitting model. Such a fudge is unsatisfactory and indicates a failure of understanding of the data errors. However, there are grounds for suspecting that some of the published errors are too low, so ϵ is not a surprisingly large correction. There may be excessive democracy here, in that the formally most accurate data sets are penalized most strongly by this procedure. On the other hand, these may be the ones most likely to 'detect' small residual systematics; it seems conservative to distribute the blame for any small disagreement uniformly. One might also query whether this correction should be applied at all k; for many models, the disagreement is worst at high k. We shall stick with the simplest procedure, since the quoted errors are usually much larger at low k.

Of our free parameters, only two are really important: Ω and a measure of the overall level of fluctuations. We take the *IRAS* bias parameter to play this latter role. Once these two

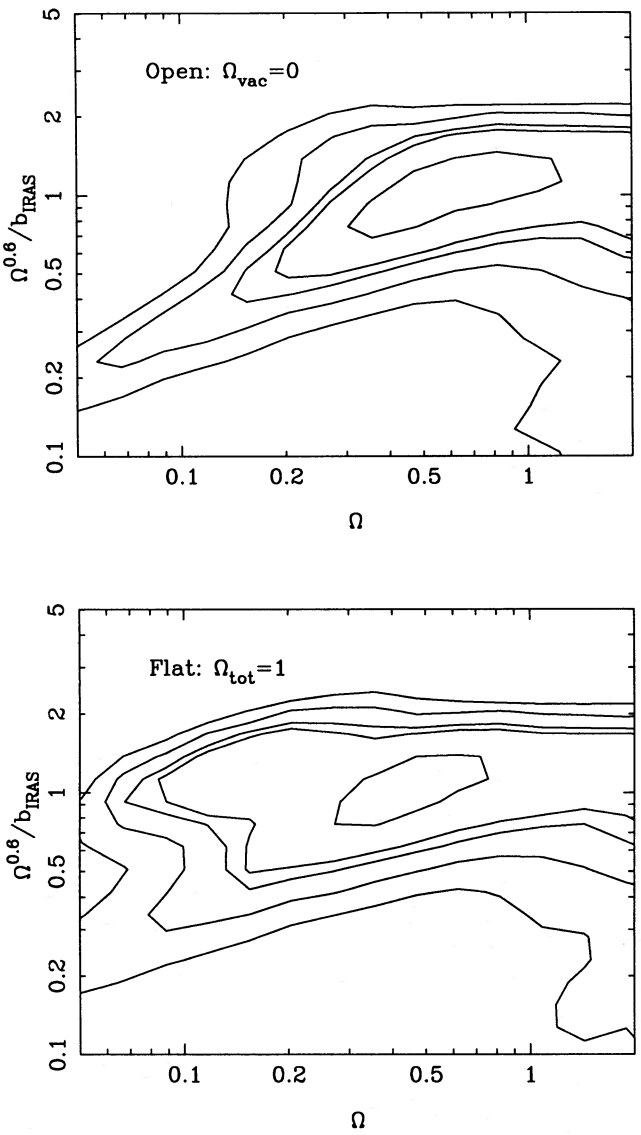

Figure 5. Contours of relative likelihood based on the degree of agreement of the various estimates of linear power spectra. At each (Ω, b_I) point, the other bias factors have been optimized. We distinguish the cases $\Omega_v = 0$ (open) and $\Omega_m + \Omega_v = 1$ (flat). Contours are plotted at what would be the 50, 90, 95, 99, 99.5 per cent confidence levels in a two-dimensional Gaussian (i.e. $\Delta \ln \mathscr{L} = 0.69, 2.3, 3.0, 4.6, 5.3$).

are specified, the other bias parameters are well determined – principally from the data at small k, where we are in the linear regime. The best-fitting values depend only very slightly on the two controlling parameters, and for all allowed models are close to

$$b_A : b_R : b_O : b_I = 4.5 : 1.9 : 1.3 : 1, \tag{38}$$

to within 6 per cent rms. We now show likelihood plots for the remaining two parameters, Ω and b_I. Contours of likelihood are displayed in Fig. 5, distinguishing the cases $\Omega_v = 0$ (open) and $\Omega_m + \Omega_v = 1$ (flat). Two main features are visible on these plots: the data appear to demand a significant degree of redshift-space distortion, with the optimal model having

$$\frac{\Omega^{0.6}}{b_I} = 1.0 \pm 0.2 \tag{39}$$

in both cases (rms error). Models satisfying this constraint in which both Ω and b_I are large are allowed, corresponding to models well in the linear regime. However, low-bias models appear to be less favoured: for low Ω, the best models have $b_I \simeq 0.8$. For the case of flat models, there is a certain bimodality, with the preferred values of b_I for $\Omega = 0.1$ being 0.8 and 0.25. However, the heavily antibiased branch of solutions can probably be excluded on other grounds, and we ignore it hereafter. At the 90 per cent confidence level, this analysis requires $\Omega > 0.14$. The various reconstructions of the linear power spectrum for the case $\Omega = b_I = 1$ are shown superimposed in Fig. 6, and display an impressive degree of agreement. This argues very strongly that what we measure with galaxy clustering has a direct relation to mass fluctuations, rather than the large-scale clustering pattern being an optical illusion caused by non-uniform galaxy-formation efficiency (Bower et al. 1993). If this were the case, the spectrum inferred from clusters should have a very different shape at large scales, contrary to observation.

The detection of redshift-space distortions is based largely on the inclusion of the APM survey, since it is the only real-space measurement used here. If this data set is removed from the analysis, small values of $\Omega^{0.6}/b_I$ are no longer excluded. An upper limit at $\Omega^{0.6}/b_I \lesssim 2$ can still be set; this comes primarily from the cross-correlation data. In real space, the cross-correlation should be the geometric mean of the two autocorrelation results. Because of the different effects of the redshift-space mapping, however, this is no longer true when redshift-space distortions become large. The observed cross-correlations thus set a limit to how strong the distortion can be. Some independent confidence in the detection of non-zero distortion can be gained from the work of Saunders, Rowan-Robinson & Lawrence (1992). They deduced the real-space correlation function for *IRAS* galaxies: $\xi(r) = (r/r_0)^{-\gamma}$, with $r_0 = 3.78 \pm 0.14\, h^{-1}$Mpc and $\gamma = 1.57 \pm 0.03$. If we convert this to a power spectrum, it lies lower than the QDOT results of FKP by a factor 1.61 ± 0.26 over the range $0.05h < k < 0.15h$ Mpc^{-1}. This corresponds to $\Omega^{0.6}/b_I = 0.75 \pm 0.25$, in good agreement with the figure deduced above, and provides independent evidence for the detection of significant redshift-space distortion. This lower degree of real-space clustering is also in agreement with our ratio of 1.3 between optical and *IRAS* bias factors. The Saunders et al. figure for r_0 predicts $r_0 = 5.3\, h^{-1}$Mpc for optically selected galaxies in real space, which is very close to the canonical value. *IRAS* galaxies have a slightly smaller value of γ, but this only produces an important change in relative power on scales rather smaller than those probed here.

The conclusion that models with $\Omega^{0.6}/b_I \simeq 1$ and low Ω are not allowed stems from the effect of non-linearities: the true level of mass fluctuations in such models would be very high. Moreover, a decrease of Ω increases the effect of non-linearities, as discussed above; this trend is less marked for the flat models, which is why low densities are not so strongly excluded in that case. It is easy to see how this conclusion arises by referring to Fig. 6. This shows that the linear power spectra inferred from galaxy and cluster data agree down to $k \simeq 0.3\, h\,$Mpc^{-1}, where $\Delta^2 \simeq 1$ in the best-fitting case. If we assume a higher normalization, the effect of non-linearities in this case is to add

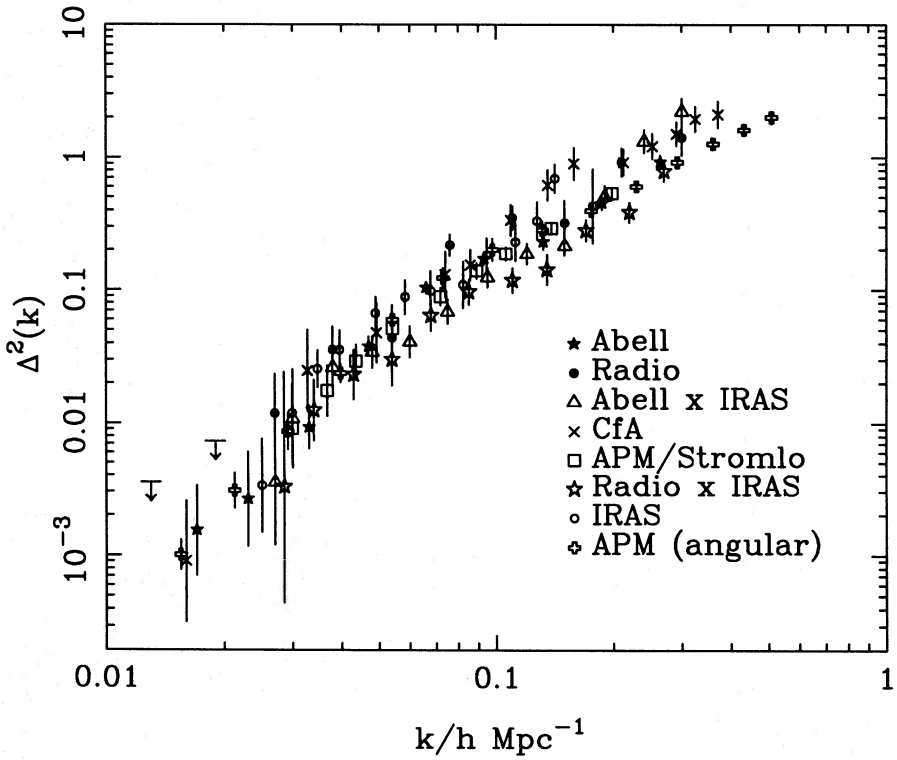

Figure 6. The power-spectrum data from Fig. 4, individually linearized assuming $\Omega = b_I = 1$. There is an excellent degree of agreement, particularly in the detection of a break around $k = 0.03h$.

power, so the linear reconstruction from galaxy data would become very flat at high k (cf. Fig. 3). However, this would disagree with the cluster data, which would still indicate a steep power spectrum, since we have assumed that the clusters give the linear result directly. This is a general problem with highly evolved models: since non-linearities change the shape of the power spectrum at $\Delta^2 \simeq 1$, and especially so for low densities, it requires something of a conspiracy for the non-linear power spectrum to be a featureless power law (see Gott & Rees 1975). However, on the present assumptions, extreme non-linear evolution should steepen the galaxy correlations faster than those for clusters, and yet they empirically have much the same slope. The easiest way of understanding this is to say that the degree of non-linearity is only mild. This is certainly an issue which merits further investigation, and a detailed simulation of cluster formation in a highly non-linear low-density model would be most valuable. In the meantime, it is interesting to note that the constraints we have drawn here on density and bias are very similar to those obtained in a completely independent way by the POTENT group in their analysis of the peculiar-velocity field (Dekel et al. 1993).

Table 1 gives the final data for the mean reconstructed power spectrum, for the case $\Omega = b_I = 1$. The data have been averaged in bins of width 0.1 in $\log_{10}$(wavenumber) and the errors quoted are standard errors. These numbers are plotted in Fig. 7, and will be compared with models in the next section; as will be shown there, the data are consistent with a smooth and featureless power spectrum, despite the small size of the errors. One of the pleasant features of our result is that the power spectrum is only weakly dependent on model parameters. For $\Omega = 1$, the power is not so sensitive to b, because in redshift space (the majority of the data) we measure

$$\Delta_z^2 \propto b^2 \left(1 + \frac{2}{3}[f/b] + \frac{1}{5}[f/b]^2\right). \tag{40}$$

The overall power correction factor thus scales only as $b^{10/7}$ for b close to unity. This can be used to rescale our 'standard' result to some other desired value of b, given $\Omega = 1$. For low densities, an empirical formula for the scaling of the linear mass spectrum in the present analysis is

$$\Delta_L^2 \propto \Omega^{-0.3}. \tag{41}$$

It is convenient to be able to compare the results here with another common measure of the amplitude of linear mass fluctuations. This is σ_8: the linear-theory rms density contrast when averaged over spheres of radius $8\,h^{-1}$ Mpc:

$$\sigma_R^2 = \int \Delta^2(k)\,\frac{dk}{k}\,\frac{9}{(kR)^6}[\sin kR - kR\cos kR]^2. \tag{42}$$

The squared window function weighting the power spectrum is very close to a Gaussian $W_k^2 = \exp[-k^2R^2/5]$, and so σ_R^2 is just $\Delta^2(k)$ at some effective wavenumber:

$$\sigma_R^2 = \Delta^2(k_R), \tag{43}$$

$$k_R = \left[\frac{([n+1]/2)\,!}{2}\right]^{1/(n+3)} \frac{\sqrt{5}}{R}, \tag{44}$$

where n is the effective power-law index of the power spectrum. As before, this approximation is within a few per cent of the exact integration provided that $n \lesssim 0$. On the scales of

Table 1. The linear power-spectrum data, assuming $\Omega = b_1 = 1$. To scale the data to other values of these parameters, see Section 5.2.

$k/h\,\mathrm{Mpc}^{-1}$	$\Delta^2(k)$	$\pm$
0.014	0.0010	0.0003
0.018	0.0013	0.0008
0.022	0.0032	0.0009
0.028	0.0087	0.0023
0.035	0.0196	0.0037
0.045	0.0312	0.004
0.056	0.052	0.008
0.071	0.107	0.011
0.089	0.146	0.017
0.112	0.211	0.027
0.141	0.33	0.033
0.178	0.43	0.051
0.224	0.73	0.095
0.282	1.14	0.13
0.355	1.63	0.27
0.447	1.61	0.41

interest, the effective index is close to -1.5 and so the effective wavenumber for σ_8 is $k = 0.20$. Using the above scalings, we get

$$\sigma_8 = 0.75\,\Omega^{-0.15}, \tag{45}$$

with a formal rms uncertainty of 13 per cent.

The significance of $8\,h^{-1}$ Mpc as a normalization scale is that σ_8 is of order unity and thus its value can be probed by observations of weakly non-linear structures such as galaxy clusters. White, Efstathiou & Frenk (1993) discuss this constraint, and deduce $\sigma_8 = 0.57\,\Omega^{-0.56}$ for spatially flat models (although the scaling should be very similar for open models), to within a tolerance of roughly ± 10 per cent. The precise meaning of their uncertainty is hard to quantify, but it seems intended to give hard limits, rather than an rms. The agreement with our results is very good; the Ω dependence is steeper, but the disagreement in σ_8 is only a factor 1.4 even for $\Omega = 0.2$.

6 POWER-SPECTRUM DATA AND MODELS

6.1 CDM-like models

It is interesting to ask if the power spectrum contains any features, or whether it is consistent with a single smooth curve. In fact, a variety of simple models describe the data from Table 1 very well within the errors. Consider the fitting formula used by Peacock (1991), which is just a break between two power laws:

$$\Delta^2(k) = \frac{(k/k_0)^\alpha}{1 + (k/k_\mathrm{c})^{\alpha-\beta}}. \tag{46}$$

This works well, with

$$k_0 = 0.29 \pm 0.01\ h\,\mathrm{Mpc}^{-1}, \tag{47}$$

$$k_1 = 0.039 \pm 0.002\ h\,\mathrm{Mpc}^{-1}, \tag{48}$$

$$\alpha = 1.50 \pm 0.03, \tag{49}$$

$$\beta = 4.0 \pm 0.5. \tag{50}$$

A value of $\beta = 4$ corresponds to a scale-invariant spectrum at large wavelengths.

A more physical alternative is the CDM power spectrum, which is $\Delta^2(k) \propto k^{n+3} T_k^2$. We shall use the BBKS approximation for the transfer function:

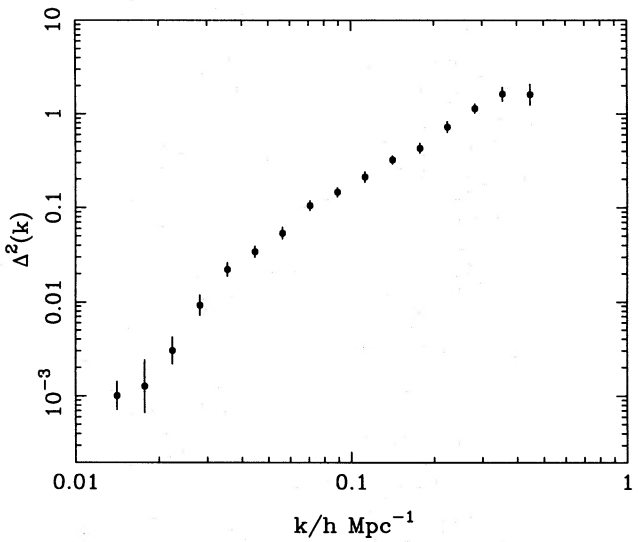

Figure 7. The linearized data of Fig. 6, averaged over bins of width 0.1 in $\log_{10} k$. This plot assumes $\Omega = b_1 = 1$; for lower densities the power increases slightly, as described in the text.

$$T_k = \frac{\ln(1 + 2.34q)}{2.34q} \times [1 + 3.89q + (14.1q)^2 + (5.46q)^3 + (6.71q)^4]^{-1/4}, \tag{51}$$

where $q \equiv k/[\Omega h^2\ \mathrm{Mpc}^{-1}]$. Since observable wavenumbers are in units of $h\,\mathrm{Mpc}^{-1}$, the shape parameter is the apparent value of Ωh. This scaling applies for models with zero baryon content, but there is an empirical scaling that can account for the effect of baryons, and which deserves to be more widely known. Fig. 8 shows a compilation of CDM transfer functions taken from Holtzman (1989). When plotted against $k/\Omega h^2$, there is a strong dependence on baryon density: high baryon content mimics low CDM density. If we instead use the scaling

$$T_k(k) = T_\mathrm{BBKS}(k/[\Omega h^2 \exp(-2\Omega_\mathrm{B})]), \tag{52}$$

then all the curves lie on top of one another to a few per cent tolerance. We shall henceforth use the term 'Ωh' to refer to the BBKS fitting parameter, on the understanding that it means the combination $\Omega h \exp(-2\Omega_\mathrm{B})$. Our results will hence differ slightly from those of Efstathiou, Bond & White (1992), who defined a parameter Γ which is almost Ωh. Unfortunately, they scaled to a 'standard' CDM model with $\Omega_\mathrm{B} = 0.03$, with the result that $\Gamma = 1.06\Omega h$.

Fitting of the CDM model to our data also results in a satisfactory χ^2 and requires the parameters

$$\Omega h = 0.255 \pm 0.017 + 0.32(1/n - 1), \tag{53}$$

in agreement with many previous arguments suggesting that a low-density model is needed. The fit of this and other models is illustrated in Fig. 9. For any reasonable values of h and baryon density, a high-density CDM model is not viable. Even a high degree of 'tilt' in the primordial spectrum (Cen et al. 1992) does not help reach the required $\Omega h \simeq 0.75$. The alternatives are to retain the CDM model, but assume that some piece of unknown physics has produced a transfer function that looks like a low-density model, or to adopt a low density, or to go for

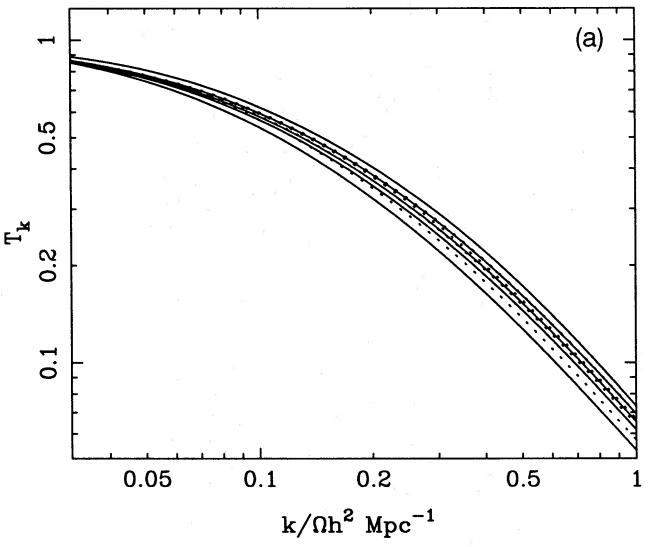

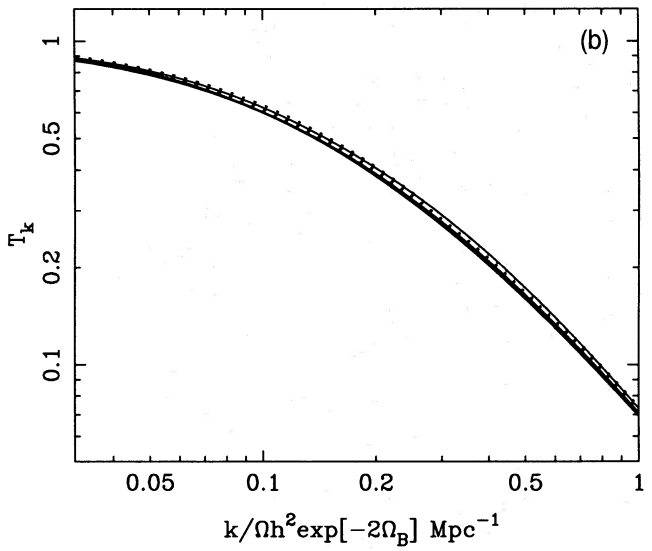

Figure 8. A set of CDM transfer functions, using the fitting formulae of BBKS for zero baryon content, and those of Holtzman (1989) for $\Omega_B = 0.01, 0.03, 0.05, 0.1$. Models with $h = 1$ are shown as solid lines, $h = 0.5$ are dotted. When plotted (panel a) against $k/\Omega h^2$, the varying baryon content causes variations in the curves, with higher Ω_B producing greater suppression of power. However, this can be scaled away (panel b) by plotting against the combination $k/[\Omega h^2 \exp(-2\Omega_B)]$. In these terms, the CDM transfer function has a universal shape, which can be described by the zero-baryon formula of BBKS. The scaling becomes noticeably imperfect for $\Omega_B \gtrsim 0.3$, but is very good for the models plotted here.

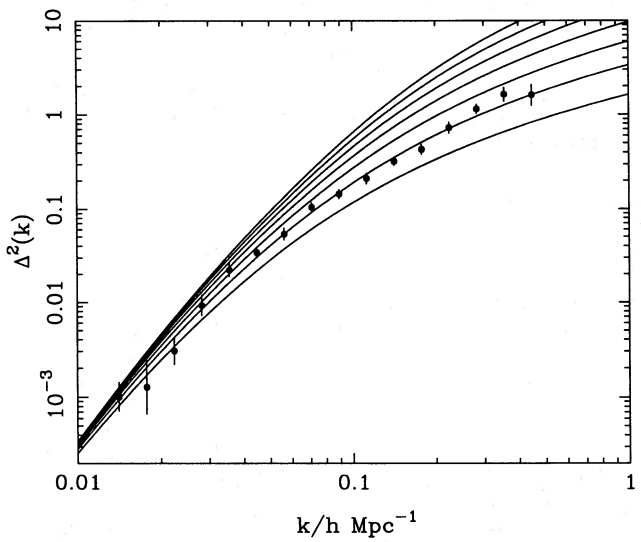

Figure 9. The averaged linear power-spectrum data of Fig. 7, compared to various CDM models. These assume scale-invariant initial conditions, with the same large-wavelength normalization. Different values of the fitting parameter $\Omega h = 0.5, 0.45, \ldots 0.25, 0.2$ are shown; power is an increasing function of Ωh, so that the 'standard' $\Omega h = 0.5$ model has the highest power, whereas $\Omega h = 0.2$ has the lowest. The best-fitting model has $\Omega h = 0.25$ and a normalization which is 1.5σ higher than *COBE* if $\Omega = 1$ and gravity-wave anisotropies are negligible ($\epsilon = 3.25 \times 10^{-5}$).

something else entirely. As far as low densities are concerned, note that the popular choice of $\Omega = 0.2$ (e.g. Kauffmann & White 1992) will overshoot and yield too low values of Ωh. More viable alternatives with high density are either mixed dark matter (MDM: Holtzman 1989; van Dalen & Schaefer 1992; Taylor & Rowan-Robinson 1992; Davis, Summers & Schlegel 1992; Klypin et al. 1993; Pogosyan & Starobinsky 1993), or non-Gaussian pictures such as cosmic strings + hot dark matter, where the lack of a detailed prediction for the power spectrum helps ensure that the model is not yet excluded (Albrecht & Stebbins 1992). Mixed dark matter seems rather ad hoc, but may be less so if it is possible to produce both hot and cold components from a single particle, with a Bose condensate playing the role of the cold component (Madsen 1992; Kaiser, Malaney & Starkman 1993). However, the shape of the MDM spectrum is not very close to the spectrum deduced here: it bends much more sharply, and is very flat on small scales. At the quasi-linear scale $k = 0.2\,h$ Mpc^{-1}, the local power-law index for the MDM model is about $n = -2.2$, as opposed to our empirical value $n \simeq -1.5$. If the good fit of a low-density CDM transfer function is taken literally, then perhaps this is a hint that the epoch of matter–radiation equality needs to be delayed. An approximate doubling of the number of relativistic degrees of freedom would suffice – but this would do undesirable violence to primordial nucleosynthesis: any such boost would have to be provided by a particle that decays after nucleosynthesis. The apparent value of Ωh depends on the mass and lifetime of the particle roughly as

$$\Omega h|_{\rm apparent} = \Omega h\,[1 + (m_{\rm keV}\tau_{\rm years})^{2/3}]^{-1/2} \qquad (54)$$

(Bardeen, Bond & Efstathiou 1987; Bond & Efstathiou 1991), so a range of masses is possible. Apart from making the observed large-scale structure, such a model yields a small-scale enhancement of power which could lead to early galaxy formation. Whether the required particle physics is at all plausible remains to be seen, but the model is arguably the most attractive of those currently available.

An important general lesson to be drawn from this section is the lack of large-amplitude features in the power spectrum.

This is a strong indication that collisionless matter is deeply implicated in forming large-scale structure. Purely baryonic models contain large bumps in the power spectrum around the Jeans length prior to recombination ($k \sim 0.03\,\Omega h^2$ Mpc^{-1}), whether the initial conditions are isocurvature or adiabatic (e.g. section 25 of Peebles 1993). It is hard to see how such features can be reconciled with the data.

6.2 Peculiar velocities

The mass power spectrum has a direct application in predicting the cosmological peculiar-velocity field. The 3D rms velocity for clumps averaged over some window is

$$\sigma_v^2 = H^2 f(\Omega)^2 \int \Delta^2(k)\,\frac{dk}{k^3}\,W_k^2, \tag{55}$$

so we can use the power spectrum to make a direct prediction of this quantity, which is shown in Fig. 10 for the case of spheres of varying radii. The velocity power spectrum ($\propto k^{-2}\Delta^2(k)$) peaks around the break in the power spectrum at $k \simeq 0.03\,h$ Mpc^{-1}, and so the predicted velocities decline rapidly for spheres which filter out this scale.

For $\Omega = 1$, the predicted velocities are very reasonable. If we model the Local Group as a sphere of radius $5\,h^{-1}$ Mpc, the 3D rms is 680 km s^{-1}, as against the observed 600 km s^{-1} one-point local measurement (the answer is very insensitive to the size used to define the Local Group). Fig. 10 also shows the deduced velocities from the POTENT group (Bertschinger et al. 1990) for spheres of radius 40 and 60 h^{-1}Mpc, which also agree well. However, the predictions are completely inconsistent with the velocity of 842 km s^{-1} for the local sphere out to $150\,h^{-1}$Mpc claimed by Lauer & Postman (1993). The predicted 3D rms for this scale is only 140 km s^{-1}. Even if we allow that their weighting scheme might reduce the effective radius of their sphere (they weight each radial shell equally), there remains a qualitative discrepancy. If this result were to be confirmed, it would probably indicate a large feature in the power spectrum on scales beyond those probed here ($k \lesssim 0.01\,h$ Mpc^{-1}).

The empirical power spectrum deduced here thus seems to agree extremely well with large-scale velocity data. The crucial test for $\Omega = 1$ models, however, has often been the small-scale velocity dispersion. The preferred low-Ωh model predicts a pairwise dispersion at $1\,h^{-1}$ Mpc separation of about $\sigma_\parallel = 550$ km s^{-1} (Mann 1993), which is interestingly close to more recent observational data (Mo et al. 1993b).

6.3 CMB anisotropies

We now relate the measurement of mass fluctuations on scales of several hundred Mpc to those implied on larger scales from the measurement of cosmic microwave background (CMB) fluctuations by the *COBE* team (Smoot et al. 1992). This is a subject which has advanced rapidly since the original detection, with a more widespread appreciation of the possible contribution of gravitational waves to the anisotropy (following the original insight of Starobinsky 1985). We therefore distinguish explicitly between scalar and tensor contributions to the CMB fluctuations by using appropriate subscripts. The former category are those described by the Sachs–Wolfe effect, and are gravitational potential fluctuations that relate directly

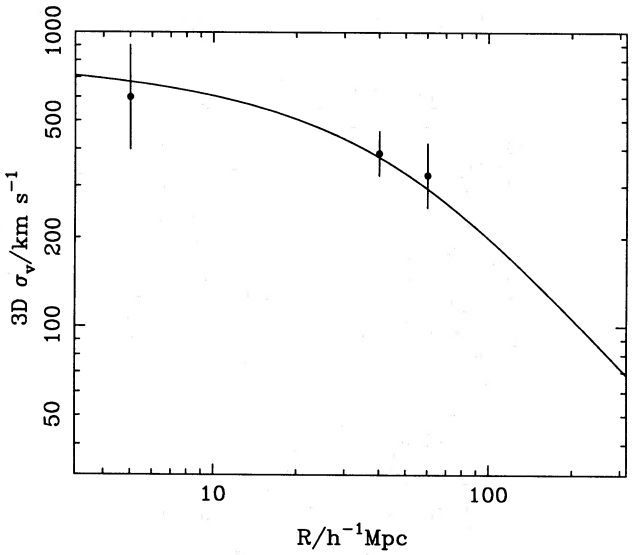

Figure 10. The predicted 3D rms velocity of spheres as a function of radius, assuming $\Omega = 1$. This is based on the two-power-law fitting formula for the power spectrum. For low densities the velocities are reduced, but by less than the normal $\Omega^{0.6}$ factor, because the inferred mass fluctuations rise in that case (see text). The plotted points are the Local Group motion assigned to a radius of $5\,h^{-1}$Mpc, and motion of larger spheres taken from the POTENT group (Bertschinger et al. 1990). Although the Local Group motion is very well determined, it is assigned a fractional error of $6^{-1/2}$ to allow for fluctuations in the 3D rms velocity seen by different observers.

to mass fluctuations. For a Gaussian beam of FWHM 2.35σ, the correlation function of the microwave sky is

$$C_s(\theta) = \frac{1}{4\pi}\sum_\ell (2\ell+1)\,W_\ell^2\,C_\ell\,P_\ell(\cos\theta), \tag{56}$$

where P_ℓ are Legendre polynomials, and $W_\ell = \exp(-\ell^2\sigma^2/2)$. The coefficients C_ℓ are

$$C_\ell = 16\pi\,\frac{\Omega^2}{g^2(\Omega)}\int (k[2c/H_0])^{-4}\Delta^2(k)\,j_\ell^2(kR_H)\,\frac{dk}{k}, \tag{57}$$

where j_ℓ are spherical Bessel functions (see Peebles 1982). The length R_H is the present comoving horizon size

$$R_H = \frac{2c}{\Omega H_0} \quad \text{(open)} \tag{58}$$

$$\simeq \frac{2c}{\Omega^{0.4} H_0} \quad \text{(flat)} \tag{59}$$

(Vittorio & Silk 1991) and the function $g(\Omega)$ is the linear growth suppression factor relative to $\Omega = 1$, as discussed earlier. These formulae strictly apply only to spatially flat models, since the notion of a scale-free spectrum is imprecise in an open model. Nevertheless, since the curvature radius subtends an angle of $\Omega/[2(1-\Omega)^{1/2}]$, normalization to *COBE* in an open model should not be a very bad approximation until we reach $\Omega \lesssim 0.2$. We shall therefore ignore this uncertainty in what follows. We also ignore corrections to the first few multipoles which arise through the time dependence of the gravitational potential in flat vacuum-dominated models (Kofman et al. 1993).

In the case of the *COBE* measurements, the simplest and most robust datum is just the sky variance convolved to 10° FWHM, i.e. $C_S(0)$ in the above expression with $\sigma = 4.^\circ25$. This can be converted into an integral over the power spectrum multiplied by a window function that is a sum over Bessel functions. In practice, it is convenient to have a simpler expression for the window, and it turns out that this can be achieved to almost perfect accuracy by using a small-angle approximation:

$$C_S(0) = \frac{\Omega^2}{g^2(\Omega)} \int 4(k[2c/H_0])^{-4}\Delta^2(k)\, W^2(kR_H)\, \frac{dk}{k}, \quad (60)$$

$$W^2(y) = [1 - j_0^2(y) - 3j_1^2(y)]\, F(y\sigma)/(y\sigma), \quad (61)$$

where $F(x)$ is Dawson's integral. The terms involving Bessel functions correspond to the subtraction of monopole and dipole terms. The window function is relatively sharply peaked and so the *COBE* variance essentially picks out the power at a given scale. For the case of $\sigma = 0.0742$ (FWHM of 10°), the result is very well fitted by

$$C_S(0) = 1.665 \frac{\Omega^2}{g^2(\Omega)} [4(k_S[2c/H_0])^{-4}\Delta^2(k_S)], \quad (62)$$

$$k_S R_H = 7.29 + 2.19(n-1). \quad (63)$$

The observed value is $C^{1/2}(0) = 1.10 \pm 0.18 \times 10^{-5}$ (Smoot et al. 1992). For scale-invariant spectra, this corresponds to an rms quadrupole of $Q_{rms} = 15.0 \pm 2.5\ \mu$K. For $\Omega = 1$, this translates to a normalization of $\epsilon = 2.6 \pm 0.4 \times 10^{-5}$ in the notation of Peacock (1991). How well does this amplitude match on to the clustering observed at 100-Mpc wavelengths? If we stick to asymptotically scale-invariant spectra, the agreement is very good. The CDM fit shown in Fig. 9 requires

$$\epsilon = 3.25 \pm 0.18 \times 10^{-5}. \quad (64)$$

This is slightly higher than the *COBE* measurement, but well within experimental error. If the large-scale normalization is forced to be $\epsilon = 2.6 \times 10^{-5}$, the best-fitting CDM shape changes to $\Omega h = 0.31$. In fact, a more detailed analysis of the *COBE* data by Wright et al. (1994) yields a preferred amplitude somewhat higher than the above simple calculation, and in extremely good agreement with the fit derived from Fig. 9.

For a more general comparison, it is convenient to define a reference datum at the largest scale where our data are still accurate. From Table 1, we take this to be $\Delta^2(k = 0.028h) = 0.0087 \pm 0.0023$. At this point, there is still some curvature in the power spectrum: the $\Omega h = 0.25$ transfer function is $T_k = 0.61$ and the effective transfer function defined by the two-power-law formula is $T_k = 0.80$. We shall adopt a compromise T_k=0.70 and hence deduce

$$\Delta^2(k = 0.028h) = 0.018 \pm 0.0023 \quad (65)$$

as our best estimate of the true level of any primordial power-law fluctuations on these scales (subject to scalings as above if $\Omega \neq 1$). We can now use our earlier discussion of the *COBE* data to predict this small-scale fluctuation, ignoring for the moment any gravity-wave contribution. The answer is

$$\Delta^2(k = 0.028h) = 0.014 \exp[3.2(n-1)]\, \Omega^{-0.7} \quad \text{(open)} \quad (66)$$

$$= 0.014 \exp[3.2(n-1)]\, \Omega^{-1.6} \quad \text{(flat)}. \quad (67)$$

Thus, if we adopt $\Omega = 1$, there is a very good agreement with scale-invariance: $n = 1.08 \pm 0.04$. Conversely, tilted models do not match large and small scales very well: for $n = 0.7$, the predicted power near 100 Mpc is too small by a factor 3. Things get worse if gravity waves are included: a prediction of many inflationary models is that

$$\frac{C_\ell^G}{C_\ell^S} \simeq 6(1-n) \quad (68)$$

(e.g. Liddle & Lyth 1992; Lidsey & Coles 1992; Lucchin, Matarrese & Mollerach 1992; Souradeep & Sahni 1992), which decreases the predicted small-scale power by a further factor 2.8 for $n = 0.7$, making a total mismatch of a factor 8. It is inconceivable that our analysis of the 100-Mpc-scale power could be in error by this amount. Thus, although tilted models may be attractive in removing the one-degree 'bump' in the predicted microwave sky (Crittenden et al. 1993) and allowing consistency with intermediate-scale CMB experiments, it seems implausible that this can be the correct solution, at least if $\Omega = 1$. To allow a tilted model with $n = 0.7$, we need $\Omega \simeq 0.06$ and 0.3 respectively in the open and flat cases.

7 SUMMARY

We have analysed a compilation of recent measures of galaxy clustering, under the assumption of underlying Gaussian mass fluctuations. We have presented new methods for dealing analytically with the modifying effects of non-linear evolution and redshift-space distortions, and their effect on the power spectrum. Application of these methods to the data leads to a consistent determination of the linear mass spectrum, with the following properties.

(i) The relative bias factors for Abell clusters, radio galaxies, optical galaxies and *IRAS* galaxies must be in the ratios $b_A : b_R : b_O : b_I = 4.5 : 1.9 : 1.3 : 1$, to within 6 per cent rms.

(ii) The data require a significant degree of redshift-space distortion: $\Omega^{0.6}/b_I = 1.0 \pm 0.2$.

(iii) Low values of Ω and bias are disfavoured because non-linear evolution would spoil the agreement in shape between galaxy and cluster power spectra. Both this and the previous conclusion are in good agreement with independent studies based on peculiar-velocity fields.

(iv) The linear power spectrum is smooth and featureless, and is well described by a zero-baryon CDM model with $\Omega h = 0.25$.

(v) The amplitude of 100-Mpc power matches well to that inferred from *COBE* provided that the primordial spectrum was close to scale-invariant. Tilted models that postulate a dominant gravity-wave CMB component are difficult to reconcile with our data.

ACKNOWLEDGMENTS

SJD is supported by a SERC research studentship. We thank Hugh Couchman for the use of his AP^{3}M code, Carlton Baugh for communicating the APM power-spectrum data, and Guinevere Kauffmann & Simon White for providing N-body data.

REFERENCES

Albrecht A., Stebbins A., 1992, Phys. Rev. Lett., 69, 2615
Babul A., Postman M., 1990, ApJ, 359, 280

Bardeen J.M., Bond J.R., Kaiser N., Szalay A.S., 1986, ApJ, 304, 15 (BBKS)
Bardeen J.M., Bond J.R., Efstathiou G., 1987, ApJ, 321, 28
Baugh C.M., Efstathiou G., 1993, MNRAS, 265, 145
Bertschinger E., Dekel A., Faber S.M., Dressler A., Burstein D., 1990, ApJ, 364, 370
Bond J.R., Couchman H.M.P., 1988, in Coley A., Dyer C.C., Tupper B.O.J., eds, Proc. Second Canadian Conference on General Relativity & Relativistic Astrophysics. World Scientific, Singapore, p.385
Bond J.R., Efstathiou G., 1991, Phys. Lett. B, 265, 245
Bouchet F.R., Strauss M.A., Davis M., Fisher K.B., Yahil A., Huchra J.P., 1993, ApJ, 417, 36
Bower R.G., Coles P., Frenk C.S., White S.D.M., 1993, ApJ, 405, 403
Broadhurst T.J., Ellis R.S., Koo D.C., Szalay A.S., 1990, Nat, 343, 726
Carroll S.M., Press W.H., Turner E.L., 1992, ARA&A, 30, 499
Cen R., Ostriker J.P., 1992, ApJ, 399, L113
Cen R., Gnedin N.Y., Kofman L.A., Ostriker J.P., 1992, ApJ, 399, L11
Coles P., Plionis M., 1991, MNRAS, 250, 75
Couchman H.M.P., 1991, ApJ, 368, L23
Crittenden R., Bond J.R., Davis R.L., Efstathiou G., Steinhardt P.J., 1993, Phys. Rev. Lett., 71, 324
Davis M., Efstathiou G., Frenk C.S., White S.D.M., 1985, ApJ, 292, 371
Davis M., Summers F.J., Schlegel D., 1992, Nat, 359, 393
Dekel A., Bertschinger E., Yahil A., Strauss M.A., Davis M., Huchra J.P., 1993, ApJ, 412, 1
Efstathiou G., Bond J.R., White S.D.M., 1992, MNRAS, 258, 1P
Einasto J., Jôeveer M., Saar E., 1980, MNRAS, 193, 353
Feldman H.A., Kaiser N., Peacock J.A., 1994, ApJ, in press (FKP)
Fisher K.B., Davis M., Strauss M.A., Yahil A., Huchra J.P., 1993, ApJ, 402, 42
Gaztañaga E., 1992, ApJ, 398, L17
Gooding A.K., Park C., Spergel D.N., Turok N., Gott J.R., III, 1992, ApJ, 393, 42
Gott J.R., III, Rees M.J., 1975, A&A, 45, 365
Gramann M., Cen R., Bahcall N., 1993, ApJ, 419, 440
Hamilton A.J.S., Gott J.R., III, Weinberg D.H., 1986. ApJ, 309, 1
Hamilton A.J.S., Kumar P., Lu E., Matthews A., 1991, ApJ, 374, L1 (HKLM)
Holtzman J.A., 1989, ApJS, 71, 1
Kaiser N., 1984, ApJ, 284, L9
Kaiser N., 1987, MNRAS, 227, 1
Kaiser N., Peacock J., 1991, ApJ, 379, 482
Kaiser N., Malaney R.A., Starkman G.D., 1993, Phys. Rev. Lett., 71, 1128
Kauffmann G., White S.D.M., 1992, MNRAS, 258, 511
Klypin A., Holtzman J., Primak J., Regős E., 1993, ApJ, 416, 1
Kofman L., Gnedin N., Bahcall N., 1993, ApJ, 413, 1
Kofman L., Gelb J., Bertschinger E., Nusser A., Dekel A., 1994, ApJ, in press
Lahav O., Lilje P.B., Primak J.R., Rees M.J., 1991, MNRAS, 251, 128
Lauer T.R., Postman M., 1993. Proc. Milan meeting on observational cosmology
Liddle A.R., Lyth D., 1992, Phys. Lett. B, 291, 391
Lidsey J.E., Coles P., 1992, MNRAS, 258, 57P
Loveday J., Efstathiou G., Peterson B.A., Maddox S.J., 1992, ApJ, 400, L43
Lucchin F., Matarrese S., Mollerach S., 1992, ApJ, 401, 49
Madsen J., 1992, Phys. Rev. Lett., 69, 571
Mann R.G., 1993, PhD thesis, University of Edinburgh
Mann R.G., Heavens A.F., Peacock J.A., 1993, MNRAS, 263, 798
Mo H.J., Peacock J.A., Xia X.Y., 1993a, MNRAS, 260, 121
Mo H.J., Jing Y.P., Börner G., 1993b, MNRAS, 264, 825
Moore B. et al., 1992, MNRAS, 256, 477
Nusser A., Dekel A., 1993, ApJ, 405, 437
Peacock J.A., 1991, MNRAS, 253, 1P
Peacock J.A., 1992, in Martinez V., Portilla M., Sáez D., eds, New insights into the Universe, Proc. Valencia summer school. Springer, Berlin, p.1
Peacock J.A., Heavens A.F., 1985, MNRAS, 217, 805
Peacock J.A., Nicholson D., 1991, MNRAS, 253, 307
Peacock J.A., West M.J., 1992, MNRAS, 259, 494
Peebles P.J.E., 1973, ApJ, 185, 413
Peebles P.J.E., 1980, The Large-Scale Structure of the Universe. Princeton Univ. Press, Princeton, NJ
Peebles P.J.E., 1982, ApJ, 263, L1
Peebles P.J.E., 1993, Principles of physical cosmology. Princeton Univ. Press, Princeton, NJ
Pogosyan D.Yu., Starobinsky A.A., 1993, MNRAS, 265, 507
Saunders W., Rowan-Robinson M., Lawrence A., 1992, MNRAS, 258, 134
Scherrer R.J., 1992, ApJ, 390, 330
Smoot G.F. et al., 1992, ApJ, 396, L1
Souradeep T., Sahni V., 1992, Mod. Phys. Lett., 7, 3541
Starobinsky A.A., 1985, Sov. Astron. Lett., 11, 133
Strauss M.A., Davis M., Yahil Y., Huchra J.P., 1992, ApJ, 385, 421
Szalay A.S., Ellis R.S., Koo D.C., Broadhurst T., 1991, in Holt S.S., Bennett C.L., Trimble V., eds, After the first three minutes, Proc. AIP Conf. 222. AIP, New York, p.261
Taylor A.N., Rowan-Robinson M., 1992, Nat, 359, 396
van Dalen A., Schaefer R.K., 1992, ApJ, 398, 33
Vittorio N., Silk J., 1991, ApJ, 385, L9
Vogeley M.S., Park C., Geller M., Huchra J.P., 1992, ApJ, 391, L5
Weinberg D.H., Cole S., 1992, MNRAS, 259, 652
White S.D.M., Efstathiou G., Frenk C.S., 1993, MNRAS, 262, 1023
Wright E.L. et al., 1994, COBE preprint 93–06, ApJ, in press
Zeldovich Ya.B., 1970, A&A, 5, 84

This paper has been produced using the Blackwell Scientific Publications LaTeX style file.